

¹ **neonSoilFlux: An R Package for Continuous
2 Sensor-Based Estimation of Soil CO₂ Fluxes**

³ John Zobitz¹ Edward Ayres² Zoey Werbin³ Ridwan Abdi¹
⁴ Natalie Ashburner-Wright⁵ Lillian Brown⁵
⁵ Ryan Frink-Sobierajski⁵ Lajntxiag Lee¹ Dijonë Mehmeti¹
⁶ Christina Tran⁵ Ly Xiong¹ Naupaka Zimmerman^{4,5}

⁷ ¹ Augsburg University, 2211 Riverside Avenue, Minneapolis, MN 55454

⁸ ² National Ecological Observatory Network, Battelle, 1685 38th Street, Suite 100, Boulder, CO
⁹ 80301

¹⁰ ³ Boston University, 5 Cummington Street, Boston, MA 02215

¹¹ ⁴ University of Kansas, 1450 Jayhawk Boulevard, Lawrence, KS 66045

¹² ⁵ University of San Francisco, 2130 Fulton Street, San Francisco, CA 94117

¹³ **Acknowledgments**

¹⁴ John Zobitz acknowledges Kathleen O'Rourke for code development. Naupaka Zimmerman
¹⁵ thanks technical staff at USF for support with field gear assembly and shipping. We thank the
¹⁶ NEON field staff and assignable assets teams for facilitating each of the six NEON site visits.

¹⁷ We are grateful to LI-COR technical staff for helpful discussions about optimal soil chamber
¹⁸ sampling methods. This work was supported by NSF DEB grant #2017829 awarded to John
¹⁹ Zobitz, and NSF DEB grant #2017860 awarded to Naupaka Zimmerman. This material is
²⁰ based in part upon work supported by the National Ecological Observatory Network (NEON),
²¹ a program sponsored by the U.S. National Science Foundation (NSF) and operated under
²² cooperative agreement by Battelle. We also thank the reviewers and subject editor for their
²³ constructive feedback.

²⁴ **Conflict of Interest Statements**

²⁵ None of the authors have a financial, personal, or professional conflict of interest related to this
²⁶ work.

²⁷ **Author Contributions**

²⁸ Conceptualization: John Zobitz, Naupaka Zimmerman; Methodology: Edward Ayres, John
²⁹ Zobitz, Naupaka Zimmerman; Software: John Zobitz, Naupaka Zimmerman, Zoey Werbin,
³⁰ Edward Ayres, Dijonë Mehmeti, Ridwan Abdi, Ly Xiong, Lajntxiag Lee; Validation: John
³¹ Zobitz, Naupaka Zimmerman; Formal Analysis: John Zobitz, Naupaka Zimmerman, Dijonë
³² Mehmeti, Ridwan Abdi, Ly Xiong, Lajntxiag Lee; Investigation: John Zobitz, Naupaka Zimmerman,
³³ Ryan Frink-Sobierajski, Christina Tran, Natalie Ashburner-Wright, Lillian Brown;
³⁴ Resources: John Zobitz, Naupaka Zimmerman; Data curation: John Zobitz, Naupaka Zimmerman,
³⁵ Dijonë Mehmeti, Ly Xiong; Writing – original draft: John Zobitz, Naupaka Zimmerman;
³⁶ Writing – review and editing: John Zobitz, Naupaka Zimmerman, Zoey Werbin, Edward Ayres,
³⁷ Christina Tran, Dijonë Mehmeti, Ly Xiong; Visualization: John Zobitz, Naupaka Zimmerman,

³⁸ Dijonë Mehmeti, Ridwan Abdi, Ly Xiong; Supervision: John Zobitz, Naupaka Zimmerman;
³⁹ Project Administration: John Zobitz, Naupaka Zimmerman; Funding Acquisition: John Zobitz,
⁴⁰ Naupaka Zimmerman.

⁴¹ **Data Availability**

⁴² Data available via <https://doi.org/10.5281/zenodo.17516319> (Zobitz & Zimmerman, 2025).
⁴³ Field-collected data, `neonSoilFlux` calculated outputs, and manuscript-generating code are
⁴⁴ provided within this repository.

45 **1 Abstract**

- 46 1. Accurate quantification of soil carbon fluxes is essential to reduce uncertainty in estimates
47 of the terrestrial carbon sink. However, these fluxes vary over time and across ecosystem
48 types and so it can be difficult to estimate them accurately across large scales. The flux
49 gradient method estimates soil carbon fluxes using co-located measurements of soil CO₂
50 concentration, soil temperature, soil moisture, and other soil properties. The National
51 Ecological Observatory Network (NEON) provides such data across 20 ecoclimatic domains
52 spanning the continental U.S., Puerto Rico, Alaska, and Hawai‘i.
- 53 2. We present an R software package (`neonSoilFlux`) that acquires soil environmental data
54 to compute half-hourly soil carbon fluxes for each soil replicate plot at a given terrestrial
55 NEON site. To assess the computed fluxes, we visited six focal NEON sites and measured
56 soil carbon fluxes using a closed-dynamic chamber approach.
- 57 3. Outputs from the `neonSoilFlux` showed agreement with measured fluxes (R^2 between
58 measured and `neonSoilFlux` outputs ranging from 0.12 to 0.77 depending on calculation
59 method used); measured outputs generally fell within the range of calculated uncertainties
60 from the gradient method. Calculated fluxes from `neonSoilFlux` aggregated to the daily
61 scale exhibited expected site-specific seasonal patterns.
- 62 4. While the flux gradient method is broadly effective, its accuracy is highly sensitive
63 to site-specific inputs, including the extent to which gap-filling techniques are used to
64 interpolate missing sensor data and to estimates of soil diffusivity and moisture content.
65 Future refinement and validation of `neonSoilFlux` outputs can contribute to existing
66 databases of soil carbon flux measurements, providing near real-time estimates of a critical
67 component of the terrestrial carbon cycle.

68 **1.1 Keywords**

69 Soil carbon, carbon dioxide, flux gradient, carbon cycle, field validation, soil respiration,
70 ecosystem variability, diffusion

71 **2 Introduction**

72 Soils contain the planet's largest reservoir of terrestrial carbon (Jobbág & Jackson, 2000). A
73 critical component of this reservoir is soil organic matter, the accumulation of which is influenced
74 by biotic factors such as above-ground plant inputs (Jackson et al., 2017). These inputs in
75 turn are influenced by environmental factors such as growing season length, temperature, and
76 moisture (Desai et al., 2022), which also affect the breakdown of soil organic matter and its
77 return to the atmosphere. Across heterogeneous terrestrial landscapes, the interplay between
78 these biotic and abiotic factors influence the size of the soil contribution to the terrestrial
79 carbon sink (Friedlingstein et al., 2025). However, the heterogeneity of these processes across
80 diverse ecosystems in the context of rapid environmental change leads to large uncertainty
81 about the magnitude of this sink in the future, and thus there remains a pressing need to
82 quantify changes in soil carbon pools and fluxes across scales.

83 Ecological observation networks such as the United States' National Ecological Observatory
84 Network (NEON) and others (e.g. the globally-distributed FLUXNET or the European Inte-
85 grated Carbon Observation System) present a significant advancement in the nearly continuous
86 observation of biogeochemical processes at the continental scale. Notably, at 47 terrestrial
87 sites across the continental United States that span 20 ecoclimatic domains, NEON provides
88 half-hourly measurements of soil CO₂ concentration, temperature, and moisture at different
89 vertical depths. Each of these NEON sites also encompasses measurements of the cumulative
90 sum of all ecosystem carbon fluxes in an airshed using the eddy covariance technique (Baldocchi,

91 Soil observations provided by NEON are on the same timescale and standardized with
92 eddy covariance measurements from FLUXNET. These types of nearly continuous observational
93 data (NEON and FLUXNET) can be used to reconcile differences between model-derived
94 or data-estimated components of ecosystem carbon flux (Jian et al., 2022; Luo et al., 2011;
95 Phillips et al., 2017; J. Shao et al., 2015; P. Shao et al., 2013; Sihi et al., 2016).

96 Estimated or observed soil carbon fluxes are a key metric for understanding change in soil
97 carbon pools over time (Bond-Lamberty et al., 2024). A soil carbon flux to the atmosphere (F_S ,
98 units $\mu\text{mol m}^{-2} \text{s}^{-1}$), represents the aggregate process of transfer of soil CO_2 to the atmosphere
99 from physical and biological processes (e.g. diffusion and respiration). Soil carbon fluxes can
100 be assumed to encompass soil carbon respiration from autotrophic or heterotrophic sources
101 (Davidson et al., 2006) and modeled with a exponential Q_{10} paradigm (Bond-Lamberty et al.,
102 2004; Chen & Tian, 2005; Hamdi et al., 2013).

103 One common method by which F_S is measured in the field is through the use of soil chambers
104 in a closed, well-mixed system (Norman et al., 1997) with headspace trace gas concentrations
105 measured with an infrared gas analyzer (IRGA). F_S can also be estimated from soil CO_2
106 measurements at different depths in the soil using the flux-gradient method (Maier & Schack-
107 Kirchner, 2014). Closed-chamber IRGA measurements, while being the most common method,
108 require either frequent in-person site visits or expensive and fragile automated systems. The
109 potential of the gradient method is that fluxes can be estimated from continuous data recorded
110 by robust solid-state sensors. The flux-gradient method is an approach that uses conservation of
111 mass to calculate flux at a vertical soil depth z at steady state by applying Fick's law of diffusion.
112 A simplifying assumption for the flux-gradient method is that there is no mass transfer in the
113 other spatial dimensions x and y (Maier & Schack-Kirchner, 2014). The diffusivity profile, a
114 key component of this calculation, varies across the soil depth as a function of soil temperature,
115 soil volumetric water content, atmospheric air pressure, and soil bulk density (Millington &

116 Shearer, 1971; Moldrup et al., 1999; Sallam et al., 1984).

117 Databases such as the Soil Respiration Database (SRDB) or the Continuous Soil Respiration
118 Database (COSORE) add to the growing network of resources for making collected observations
119 of soil fluxes available to other researchers (Bond-Lamberty, 2018; Bond-Lamberty et al., 2020;
120 Bond-Lamberty & Thomson, 2010; Jian et al., 2021; Jiang et al., 2024). However, these
121 databases currently encompass primarily direct soil measurements of fluxes (i.e. those using
122 methods like the closed-chamber method described above). Currently, NEON provides all
123 measurements to calculate F_S from Fick's law, but soil flux as a derived data product was
124 descoped from the initial network launch due to budget constraints (Berenbaum et al., 2015).
125 Deriving estimates of F_S using continuous sensor data across NEON sites using NEON data
126 thus remains a high priority.

127 This study describes an R software package, `neonSoilFlux`, that computes a standardized
128 estimate of F_S at all terrestrial NEON sites using the flux-gradient method. Using direct
129 chamber-based field observations of soil carbon dioxide flux from a subset of terrestrial NEON
130 sites spanning six states, we provide a direct validation of F_S from `neonSoilFlux`. While
131 open source R software tools currently exist for processing chamber-based flux measurements
132 (Jurasinski et al., 2022; Pedersen, 2024; Rheault et al., 2024; Wilson et al., 2024; Zhao, 2019),
133 to our knowledge this is the first package that incorporates NEON data directly.

134 Key objectives of this study are to:

135 1. Apply the flux-gradient method to estimate soil CO₂ flux from continuous sensor mea-
136 surements across six NEON sites.
137 2. Benchmark estimated soil carbon fluxes against field measurements (e.g. direct chamber
138 measurements of soil flux).

- 139 3. Identify sources of error in the flux-gradient approach across diverse sites in order to
140 guide future work.

141 **3 Materials and Methods**

142 **3.1 Field methods**

143 **3.1.1 Focal NEON Sites**

144 In order to acquire field data to validate model predictions of flux, we selected six terrestrial
145 NEON sites for analysis. We conducted roughly week-long field measurement campaigns at
146 these sites, which span a range of environmental gradients and terrestrial domains (Table 1).
147 SJER, SRER, and WREF were visited during May and June of 2022, and WOOD, KONZ, and
148 UNDE during May and June of 2024. Permits or waivers were sought and approved prior to
149 field work at all six sites. In 2022, research activities were conducted whole or in part on the
150 Wind River Experimental Forest within the Gifford Pinchot National Forest. No permit was
151 required for this work. Approval for research at San Joaquin Experimental Range was granted
152 by Dr. Angela White in May 2022 and for research at Santa Rita Experimental Range by
153 Dr. Mitch McClaran in May 2022. In 2024, permits were received for work at WOOD (Chase
154 Lake WMD; permit number 62515-24-020), KONZ (Konza Prairie Biological Station; permit
155 number 766), and UNDE (University of Notre Dame Environmental Research Center; permit
156 number UNDERC-2024-5).

157 **3.1.2 Soil collar placement**

158 Either one (2022 sampling campaign) or two (2024 sampling campaign) PVC soil collars (20.1
159 cm inside diameter) were installed in close proximity to the permanent NEON soil sensors at
160 each site (Figure 1). As instruments in the NEON soil sensor arrays can occasionally break
161 down or stop working, the specific soil plot where we made measurements was chosen at each
162 site in consultation with NEON staff to maximize likelihood of quality soil sensor measurements
163 during the duration of the IRGA measurements. The plot selected at each site (out of the 5 in
164 each replicate array at each site) are presented in the last column of Table 1. After installation,
165 collar(s) were left to equilibrate for approximately 24 hours prior to any measurements being
166 taken.

167 **3.1.3 Infrared gas analyzer measurements of soil CO₂ flux**

168 In 2022, we then made measurements of flux on an hourly interval for 8 hours each day.
169 Measurements were taken from roughly 8 am to 4 pm, with the time interval selected to
170 capture the majority of the diurnal gradient of soil temperature each day. These measurements
171 were made using a LI-6800 infrared gas analyzer instrument (LI-COR Environmental, Lincoln,
172 NE) fitted with a soil chamber attachment (attachment 6800-09). In 2024, we again used the
173 same LI-6800 instrument, but made half-hourly measurements over an approximately 8 hour
174 period. In addition, in 2024 we also installed a second collar and used a second instrument, an
175 LI-870 CO₂ IRGA, connected to an automated robotic chamber (LI-COR chamber 8200-104)
176 controlled by an LI-8250 multiplexer to make automated measurements. The multiplexer was
177 configured to take half-hourly measurements 24 hours a day for the duration of our sampling
178 bout at each site. Each instrument was paired with a soil temperature and moisture probe
179 (Stevens HydraProbe, Stevens Water, Portland, OR) that was used to make soil temperature
180 and moisture measurements concurrent with the CO₂ flux measurements. Chamber volumes

were set by measuring collar offsets at each site. System checks were conducted daily for the LI-6800 and weekly for the LI-8250. Instruments were factory calibrated before each field season.



Figure 1: Spatial layout of field sampling using a closed-dynamic chamber setup at a representative NEON site (KONZ). Left image shows collars (white arrows) and permanent soil sensor installation (black arrow) and right image shows the LI-6800 (foreground) and LI-8200-104 (background) instruments placed on the collars.

Table 1: Listing of NEON sites studied for field work and analysis. Site refers to NEON site codes: Santa Rita Experimental Range (SRER), San Joaquin Experimental Range (SJER), Wind River Experimental Forest (WREF), Chase Lake National Wildlife Refuge (WOOD), Konza Prairie Biological Station (KONZ), and the University of Notre Dame Environmental Research Center (UNDE). Location is reported in decimal degrees of latitude and longitude. Other abbreviations include Mean Annual Temperature (MAT); \bar{T}_S : average soil temperature during field measurements; \bar{SWC} : average soil water content during field measurements. Dates refer to field measurement dates for each site. Plot refers to the particular location in the soil sensor array (denoted as HOR by NEON) where field measurements were made.

Site	Location	Ecosystem	MAT	\bar{T}_S	MAP	\bar{SWC}	Dates	Plot
SRER	31.91068, -110.83549	Shrubland	19.3 °C	47.6 °C	346 mm	4.0%	May 29– June 1 2022	004
SJER	37.10878, -119.73228	Oak woodland	16.4 °C	41.7 °C	540 mm	1.2%	June 1–4 2022	005
WREF	45.82049, -121.95191	Evergreen forest	9.2 °C	15.3 °C	2225 mm	27.2%	June 7–9 2022	001

Table 1: Listing of NEON sites studied for field work and analysis. Site refers to NEON site codes: Santa Rita Experimental Range (SRER), San Joaquin Experimental Range (SJER), Wind River Experimental Forest (WREF), Chase Lake National Wildlife Refuge (WOOD), Konza Prairie Biological Station (KONZ), and the University of Notre Dame Environmental Research Center (UNDE). Location is reported in decimal degrees of latitude and longitude. Other abbreviations include Mean Annual Temperature (MAT); \bar{T}_S : average soil temperature during field measurements; \bar{SWC} : average soil water content during field measurements. Dates refer to field measurement dates for each site. Plot refers to the particular location in the soil sensor array (denoted as HOR by NEON) where field measurements were made.

Site	Location	Ecosystem	MAT	\bar{T}_S	MAP	\bar{SWC}	Dates	Plot
WOOD	47.1282, -99.241334	Restored prairie	4.9 °C	14.9 °C	495 mm	14.9%	June 3–9 2024	001
KONZ	39.100774, -96.563075	Tallgrass prairie	12.4 °C	23.4 °C	870 mm	23.4%	May 29– June 1 2024	001
UNDE	46.23391, -89.537254	Deciduous forest	4.3 °C	13.0 °C	802 mm	13.0%	May 22–25 2024	004

3.1.4 Post-collection processing of field data

We used LI-COR SoilFluxPro software (v 5.3.1) to assess the data after collection and to inform sampling parameters. We checked appropriateness of dead band and measurement durations using built-in evaluation tools. Based on this, the deadband period was set for 30-40 seconds, depending on the site, and the measurement duration was 180 seconds with a 30 second pre-purge and a 30 second post-purge at most sites, and a 90 second pre- and post-purge at sites with higher humidity due to recent precipitation events. We also assessed the R^2 of linear and exponential model fits to measured CO₂ to verify measurement quality.

3.2 neonSoilFlux R package

We developed an R package called `neonSoilFlux` (Zobitz et al., 2024) to compute half-hourly soil carbon fluxes and uncertainties from NEON data. The objective of the `neonSoilFlux`

195 package is a unified workflow (Figure 2) for soil data acquisition and analysis that supplements
196 the existing `neonUtilities` data acquisition R package (Lunch et al., 2025).

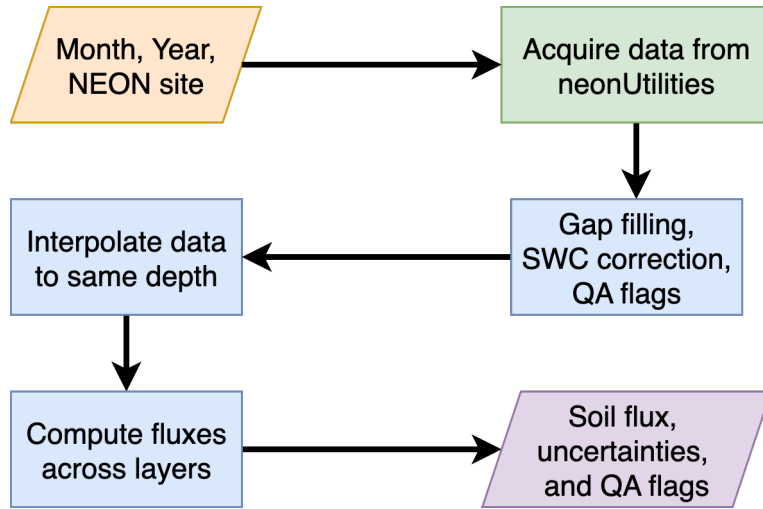


Figure 2: Diagram of `neonSoilFlux` R package. For a given month, year, and NEON site (orange parallelogram), the package acquires all relevant data to compute F_S using the `neonUtilities` R package (green rectangle). Data are gap-filled according to reported QA flags and adjusted for changes in soil water content (SWC) calibration coefficients, then interpolated to the same measurement depth before computing the soil flux, uncertainties, and final QA flags (blue rectangles). The package reports the associated soil flux, uncertainties, and quality assurance (QA) flags for the user (purple parallelogram).

197 At a given NEON site there are five replicate soil plots, each with measurements of soil
198 CO_2 concentration, soil temperature, and soil moisture at different depths (Figure 3). The
199 `neonSoilFlux` package acquires measured soil CO_2 concentration (NEON, 2024b), soil temper-
200 ature (NEON, 2024d), soil water content (NEON, 2024e), barometric pressure from the nearby
201 tower (NEON, 2024a), and soil properties (e.g. bulk density) (NEON, 2024c) from a range of
202 different NEON data products. The static soil properties were collected by NEON staff from a
203 nearby soil pit during initial site characterization and are assumed to be constant at each site.
204 A soil flux calculation is computed at each replicate soil plot.

205 The workflow to compute a value of F_S with `neonSoilFlux` consists of three primary steps,

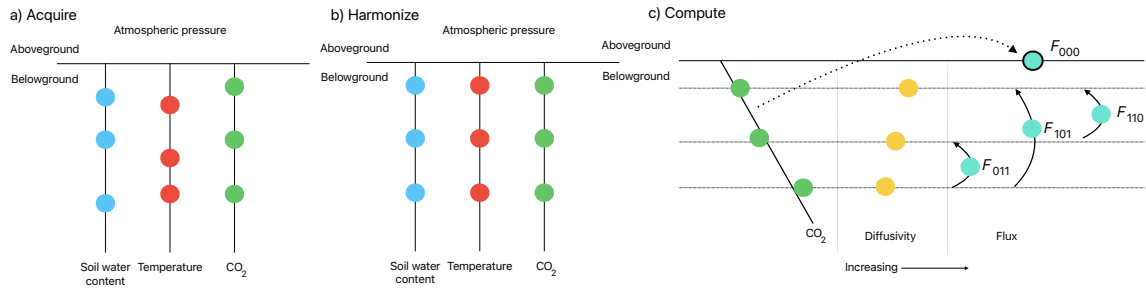


Figure 3: Model diagram of the data workflow for the `neonSoilFlux` R package. a) Acquire: Data are obtained for a given NEON location and horizontal sensor location, which includes soil water content, soil temperature, CO_2 concentration, and atmospheric pressure. All data are screened for quality assurance; if gap-filling of missing data occurs, it is flagged for the user. b) Harmonize: Any belowground data are then harmonized to the same depth as CO_2 concentrations using linear regression. c) Compute: The flux across a given depth is computed via Fick's law, denoted with F_{ijk} , where i , j , or k are either 0 or 1 denoting the layers the flux is computed across ($i =$ closest to surface, $k =$ deepest). F_{000} represents a flux estimate where the gradient dC/dz is the slope of a linear regression of CO_2 with depth.

206 illustrated in Figure 3. First, NEON data are acquired for a given site and month via the
 207 `neonUtilities` R package (yellow parallelogram and green rectangle in Figure 2 and Panel a
 208 in Figure 3). Acquired environmental data can be exported to a comma separated value file for
 209 additional analysis. Quality assurance (QA) flags are reported as an indicator variable. Since
 210 the calibration coefficients on the soil water content sensors have changed over time (NEON,
 211 2024e), raw sensor measurements were back-calculated and soil-specific calibrations were applied
 212 following Ayres et al. (2024) to generate a consistent time series at each measurement location.

213 The second step is harmonizing the data to compute soil fluxes across soil layers. This
 214 step consists of three different actions (blue rectangles in Figure 2 and Panel b in Figure 3).
 215 If a given observation by NEON is reported as not passing a quality assurance check, we
 216 applied a gap filling method to replace that measurement with its monthly mean at that same
 217 depth (Section 3.2.1). Belowground measurements of soil water and soil temperature are then
 218 interpolated to the same depth as soil CO_2 measurements. The diffusivity (Section 3.2.2) and

219 soil flux across different soil layers (Section 3.2.3) are then computed.

220 The third and final step is computing a surface soil flux through extrapolation to the surface
221 (purple parallelogram in Figure 2 and Panel c in Figure 3). Uncertainty on a soil flux
222 measurement is computed through quadrature. An aggregate quality assurance (QA) flag for
223 each environmental measurement is also reported, representing if any gap-filled measurements
224 were used in the computation of a soil flux. Within the soil flux-gradient method, several
225 different approaches can be used to derive a surface flux (Maier & Schack-Kirchner, 2014); the
226 `neonSoilFlux` package reports four different possible values for soil surface flux (Section 3.2.3)
227 for each of two different methods of diffusivity estimation, for a total of eight estimates of
228 flux.

229 3.2.1 Gap-filling routine

230 NEON reports QA flags as binary values for each measurement and half-hourly interval. For a
231 given half-hour, if any input variable (soil CO₂ concentration, soil temperature, or soil moisture)
232 at depth z is flagged, computation of F_S is not possible. To address this, flagged measurements
233 and their uncertainties were replaced with a bootstrapped monthly mean (\bar{m}) and monthly
234 standard deviation (\bar{s}) (Efron & Tibshirani, 1994).

235 For each month, depth z , and variable, we computed bootstrapped estimates of \bar{m} and \bar{s}
236 from the vectors of unflagged measurements (**m**), reported standard errors (σ), and the 95%
237 confidence interval (ϵ , or expanded uncertainty; Farrance & Frenkel (2012)). We also defined a
238 bias vector $\mathbf{b} = \sqrt{\epsilon^2 - \sigma^2}$, which quantifies the spread of uncertainty in a given period and is
239 incorporated into \bar{m} .

240 From these, 5000 bootstrap samples were generated for **m**, σ , and **b**. For each sample (m_k, b_k, σ_k),
241 we generated a vector **n** (length $N = 5000$) by drawing from a normal distribution with mean

242 $m_k + b_k$ and standard deviation σ_k . The sample mean and standard deviation were then
243 computed from \mathbf{n} . The resulting distributions of sample means and sample standard deviations
244 provided the bootstrapped monthly mean (\bar{m}) and standard error (\bar{s}) respectively.

245 This gap-filling procedure provides a consistent treatment across all data streams. However,
246 alternative approaches may be better suited for longer gaps (e.g., correlations with other NEON
247 measurement levels or soil plots) or for variable-specific conditions. We discuss the effect of
248 gap-filling on our results in Section 5.1.

249 3.2.2 Soil diffusivity

250 Soil diffusivity D_a at a given measurement depth is the product of the diffusivity in free air
251 $D_{a,0}$ ($\text{m}^2 \text{ s}^{-1}$) and the tortuosity ξ (no units) (Millington & Shearer, 1971).

252 We compute $D_{a,0}$ with Equation 1:

$$D_{a,0} = 0.0000147 \cdot \left(\frac{T_i + 273.15}{293.15} \right)^{1.75} \cdot \left(\frac{P}{101.3} \right) \quad (1)$$

253 where T_i is soil temperature ($^\circ\text{C}$) at depth i (NEON, 2024d) and P surface barometric pressure
254 (kPa) (NEON, 2024a).

255 Previous studies by Sallam et al. (1984) and Tang et al. (2003) demonstrated the sensitivity
256 of modeled F_S depending on the tortuosity model (ξ) used to compute diffusivity. At low
257 soil water content, the choice of tortuosity model can lead to order-of-magnitude differences
258 in D_a , which in turn affect modeled F_S . The `neonSoilFlux` package currently includes two
259 approaches to calculate ξ , representing the range of tortuosity behavior reported in Sallam et
260 al. (1984).

261 The first approach is the Millington-Quirk model (Millington & Shearer, 1971), in which
262 tortuosity depends on both porosity and soil water content:

$$\xi = \frac{(\phi - SWC_i)^{10/3}}{\phi^2} \quad (2)$$

263 In Equation 2, SWC is the soil water content at depth i (NEON, 2024e) and ϕ is the porosity,
264 which in turn is a function of soil physical properties (NEON, 2024c):

$$\phi = \left(1 - \frac{\rho_s}{\rho_m}\right) (1 - f_V) \quad (3)$$

265 In Equation 3, ρ_m is the particle density of mineral soil (2.65 g cm^{-3}), ρ_s the soil bulk density
266 (g cm^{-3}) excluding coarse fragments greater than 2 mm (NEON, 2024c), and f_V is a site-specific
267 value that accounts for the proportion of soil fragments between 2-20 mm. Soil fragments
268 greater than 20 mm were not estimated due to limitations in the amount of soil that can be
269 analyzed (NEON, 2024c). We assume that rock fragments contain no internal pores.

270 The Millington-Quirk model assumes ξ is modulated by the amount of fluid saturation in soil
271 pores (Millington & Shearer, 1971). In contrast, the Marshall model (Marshall, 1959) expresses
272 tortuosity as only a function of porosity ($\xi = \phi^{1.5}$), with ϕ defined from Equation 3. The
273 Marshall model is independent of soil water content and assumes tortuosity is only governed
274 by soil structure. The `neonSoilFlux` package allows users to choose the tortuosity model most
275 appropriate for site-specific conditions and research goals.

276 **3.2.3 Soil flux computation**

277 We applied Fick's law (Equation 4) to compute the soil flux F_{ij} ($\mu\text{mol m}^{-2} \text{s}^{-1}$) across two soil
278 depths i and j :

$$F_{ij} = -D_a \frac{dC}{dz} \quad (4)$$

279 where D_a is the diffusivity ($\text{m}^2 \text{s}^{-1}$) and $\frac{dC}{dz}$ is the gradient of CO_2 molar concentration (μmol
280 m^{-3} , so the gradient has units of $\mu\text{mol m}^{-3} \text{m}^{-1}$). The soil surface flux is theoretically defined
281 by applying Equation 4 to measurements collected at the soil surface and directly below the
282 surface. Measurements of soil temperature, soil water content, and soil CO_2 molar concentration
283 across the soil profile allow for application of Equation 4 across different soil depths. Each
284 site had three measurement layers, so we denote the flux as a three-digit subscript F_{ijk} with
285 indicator variables i , j , and k indicate if a given layer was used (written in order of increasing
286 depth), according to the following:

- 287 • F_{000} is a surface flux estimate using the intercept of the linear regression of D_a with
288 depth and the slope from the linear regression of CO_2 with depth (which represents $\frac{dC}{dz}$
289 in Fick's Law). Tang et al. (2003) used this approach to compute fluxes in an oak-grass
290 savannah.
- 291 • F_{110} is a flux estimate across the two shallowest measurement layers.
- 292 • F_{011} is a flux estimate across the two deepest measurement layers.
- 293 • F_{101} is a flux estimate across the shallowest and deepest measurement layers.

294 For F_{110} , F_{011} , and F_{101} , the diffusivity used in Fick's Law is always at the deeper measurement
295 layer. When used as a surface flux estimate we assume CO_2 remains constant above this flux
296 depth. Uncertainty in all F_{ijk} values was quantified using quadrature (Taylor, 2022). These

297 computed fluxes could provide the basis for additional soil flux estimates. For example, Tang et
298 al. (2005) estimated surface flux by linearly extrapolating F_{110} and F_{011} to the soil surface.

299 **3.3 Post processing evaluation**

300 Following collection of field measurements and calculation of the soil fluxes from `neonSoilFlux`
301 package, we compared measured F_S based on closed-dynamic chamber measurements with the
302 LI-COR instruments to a given soil flux calculation from `neonSoilFlux` for each site and flux
303 computation method and quantified the relationship statistically (R^2). Finally, for a half-hourly
304 interval we also computed a *post hoc* diffusivity (D_a) using the LI-COR flux along with the
305 CO_2 surface gradient reported by NEON using the measurement levels closest to the surface.

306 **4 Results**

307 **4.1 Concordance between modelled and measured soil CO_2 flux**

308 The sites we visited ranged substantially in both their annual average temperature and
309 precipitation as well as their biome type (Table 2). These differences also influenced the wide
310 range of observed flux rates across sites.

311 The timeseries of the measured fluxes from the LI-COR 6800 and 870/8250 were compared
312 to modeled soil fluxes from the `neonSoilFlux` R package (Figure 4). We also assessed year-
313 long estimated flux time series and compared those to field measurements made at each site
314 (Figure 5). Results are reported in local time. Where applicable, sites are displayed from left
315 to right by increasing soil temperature (Table 1). Positive values of the flux indicate that there
316 is a flux moving towards the surface. Overall, with the exception of SRER (discussed later) the
317 computed fluxes determined using a variety of plausible methods spanned the field-measured

Table 2: Summary of measured soil characteristics and flux results from field measurements across six NEON sites using a LI-COR 6800 (LI-870/8250 measurements omitted to enable direct comparability) via the closed-dynamic chamber method. Numeric values for soil CO₂ flux, soil temperature, and volumetric soil water content (VSWC) are the mean and standard deviation of field measurements at each site.

Site	Flux μmol m ⁻² s ⁻¹	Soil temp °C	VSWC cm ³ cm ⁻³	n
UNDE	2.55 ± 0.26	14.33 ± 0.77	0.33 ± 0.02	61
WOOD	3.02 ± 0.4	16.01 ± 1.54	0.28 ± 0.01	53
WREF	3.62 ± 0.3	15.34 ± 1.76	0.27 ± 0.06	21
KONZ	6.35 ± 0.97	27.28 ± 4.14	0.37 ± 0.01	44
SJER	0.94 ± 0.02	41.68 ± 11.22	0.01 ± 0.01	32
SRER	0.72 ± 0.09	47.64 ± 7.46	0.04 ± 0.01	32

318 fluxes, but the specific flux-gradient method that best approximated field measurements varied
319 by site.

320 We calculated a statistical relationship between the various estimates of soil flux computed by
321 `neonSoilFlux` and the field-measured fluxes within daily interval periods. Statistics for these
322 comparisons are reported in Figure 6, which also shows how these fall relative to a 1:1 line.

323 4.2 Effects of method choice on diffusivity estimates

324 In one of the six field sites, the *post hoc* D_a estimate fell roughly between the two diffusion
325 estimation methods. At UNDE, WOOD, WREF, and SJER, the median field estimate of
326 diffusivity was lower than both of the other methods. At the driest sites, SRER (Table 1),
327 the median field estimate of diffusivity was higher than both of the other methods and values
328 showed a large amount of variation (Figure 7).

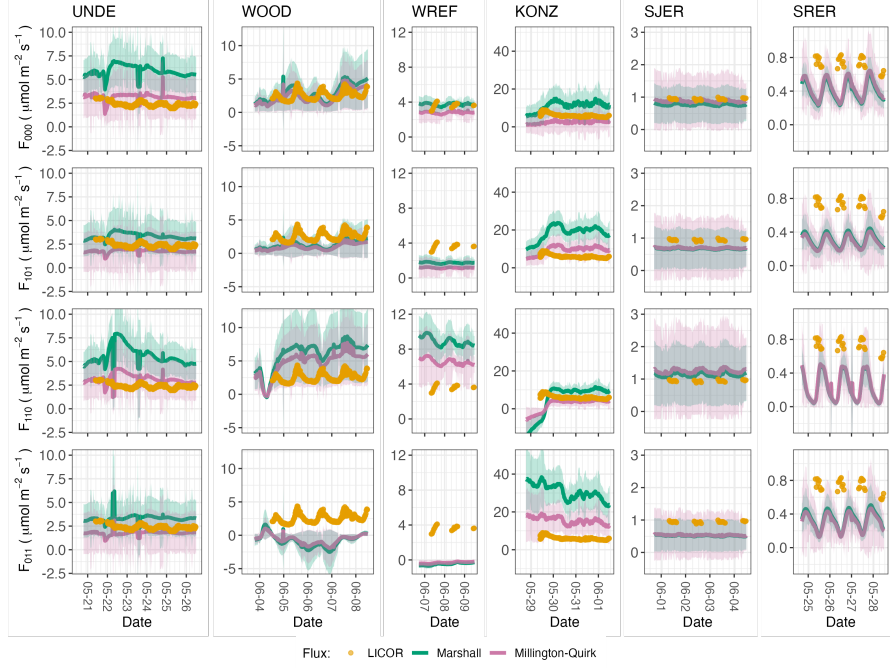


Figure 4: Timeseries of soil surface flux (F_S) from field-measured (yellow lines) and modeled soil fluxes (green or purple lines) by the `neonSoilFlux` R package. Fluxes from the `neonSoilFlux` R package are separated by the diffusivity model used (Millington-Quirk or Marshall, Section 3.2.2). Individual vertical axis labels in the first column represent the measurement levels where the flux-gradient approach is applied (Section 3.2.3). Ribbons for modeled soil fluxes represent ± 1 standard deviation. Results are reported in local time. WREF, SJER, and SRER were sampled in 2022, and UNDE, WOOD, and KONZ were sampled in 2024. Sites (columns) are arranged from left to right in terms of increasing mean annual temperature.

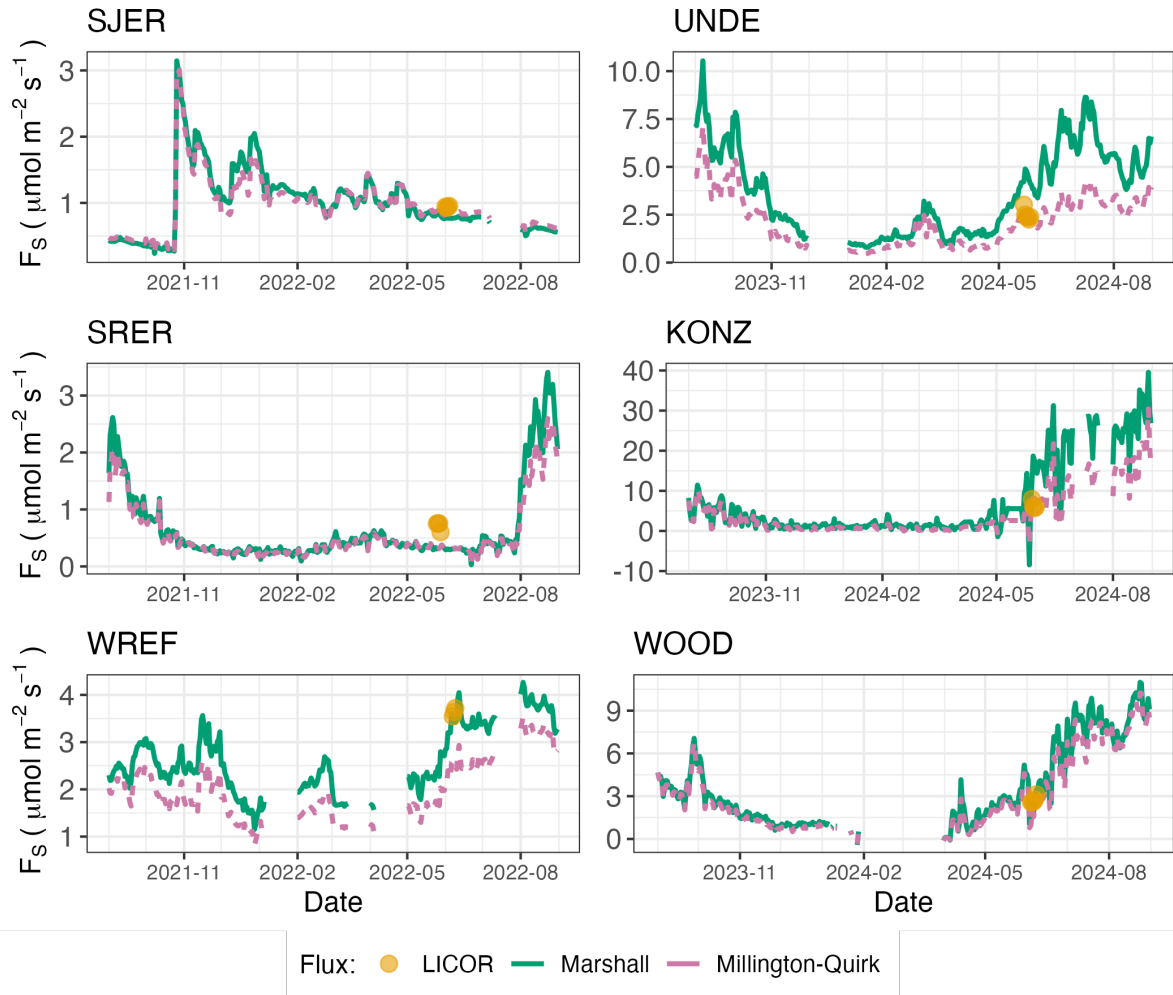


Figure 5: Timeseries of both daily-averaged field F_S (yellow circles) and daily ensemble averaged soil fluxes (average of F_{000} , F_{101} , F_{011} , F_{110} , Section 3.2.3) by the `neonSoilFlux` R package, separated by the diffusivity model used (green or purple lines, Millington-Quirk or Marshall, Section 3.2.2).

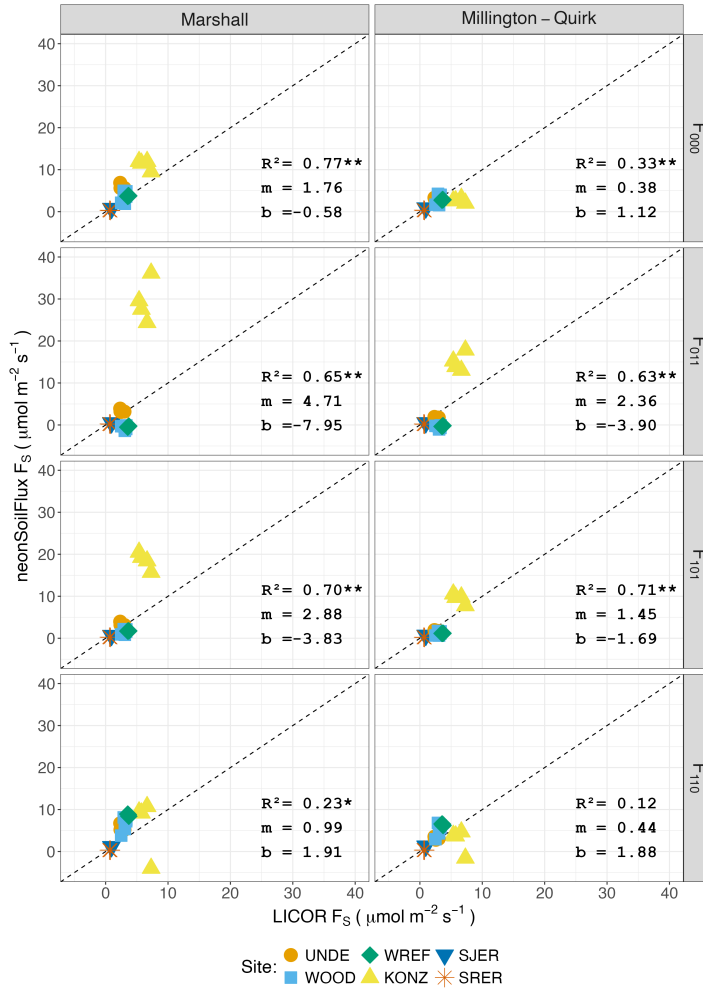


Figure 6: Statistical comparison between measured fluxes at each NEON site with fluxes reported by `neonSoilFlux` with the different flux calculation approaches and diffusivity calculations applied. Points are daily averages and LICOR F_S values are from the 6800 instrument only, for consistency. The dotted line represents a 1:1 relationship, and the reported R^2 quantifies the relationship between field-measured and `neonSoilFlux` estimated fluxes. * = significance at the 5% level, ** = significance at the 1% level. The slope (m) and intercept (b) of the linear regression between measured and modeled fluxes are also reported. The low-value outlier from KONZ in the F_{110} Marshall plot is an example of the effect of inverted CO₂ gradients causing an estimated flux to be negative, bringing down the daily mean, which later resolved as the soils dried back out.

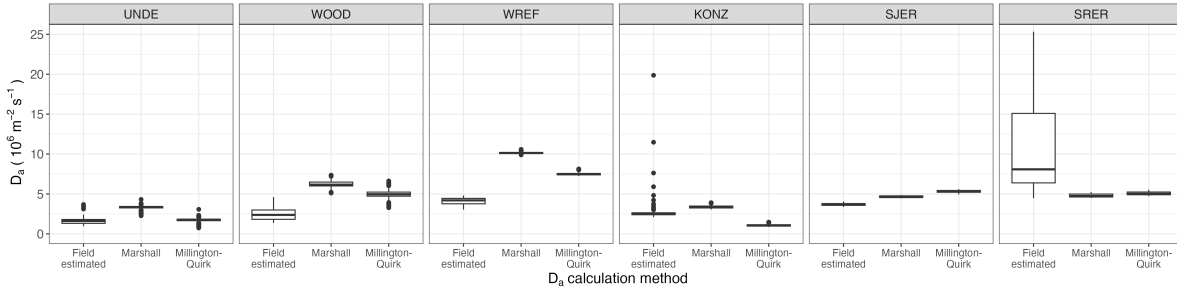


Figure 7: Distribution of diffusivity (D_a) at each study site. Values of D_a were provided by the `neonSoilFlux` package, computed from the Millington-Quirk or Marshall models (Section 3.2.2). A post-hoc estimate of diffusivity (labeled as “Field estimated”) was computed through the field measured flux (Figure 4), divided by the CO₂ gradient from the measurement levels closest to the soil surface, as reported by NEON. We only used F_S measured by the LICOR 6800 at all sites to standardize comparisons. Some outliers (n = 1 from the field estimated values at KONZ and n = 6 from field estimated values at SRER) are excluded from the plot to allow better comparative visualization across sites.

329 5 Discussion

330 This study presents a unified data science workflow to efficiently process automated measurements of belowground soil CO₂ concentrations, soil water content, and soil temperature to
 331 infer estimates of soil surface CO₂ effluxes through application of Fick’s Law (Equation 4).
 332 Our core goals in this study were: (1) to generate estimates of soil flux from continuous soil
 333 sensor data at terrestrial NEON sites using the flux-gradient method and then (2) to compare
 334 those estimates to field-measured fluxes based on the closed chamber approach at six NEON
 335 focal sites. We discuss our progress toward these core goals through (1) an overall evaluation
 336 of the flux-gradient approach (and uncertainty calculation) and (2) site-specific evaluation of
 337 differences in estimated vs measured fluxes.
 338

339 5.1 General evaluation of flux-gradient approach

340 Key assumptions of the flux-gradient approach are that CO₂ concentrations increase throughout
341 the soil profile such that the highest concentrations are observed in the deepest layers. Addition-
342 ally, field flux measurements should correlate with F_{000} because they represent surface fluxes.
343 Periods where this gradient condition are not met generally are connected to processes that occur
344 during soil wetting events, where more shallow soil layers produce higher concentrations of CO₂
345 due to microbial respiration pulses following rewetting. This effect is likely to be largest at sites
346 with rich organic soils (e.g. KONZ). Based on this reasoning, in these types of situations we would
347 *a priori* expect F_{011} (deepest layers) $\leq F_{101} \leq F_{110}$ (shallow layers) $\leq F_{000}$ (all layers) be-
348 cause the previous flux estimates rely primarily on CO₂ concentrations at deeper depths, and
349 could miss high concentrations of CO₂ produced in shallower layers.

350 When modeling soil respiration, typically a non-linear response function that also considers soil
351 type is used (Bouma & Bryla, 2000; Yan et al., 2016, 2018). For the `neonSoilFlux` package,
352 soil type is connected to the measurement of bulk density, which was characterized at each
353 NEON site. This bulk density estimate is based on replicate samples collected from the site
354 megapit at a subset of soil horizons, with an estimated uncertainty of $\pm 5\%$ (NEON, 2024c).
355 Coarse fragment estimates also have very large uncertainties, but because the volume fraction
356 tends to be low in surface soils it is unlikely to contribute much additional flux uncertainty.

357 Our results suggest that the most important way to improve reliability of the flux estimate is
358 to reduce the usage of gap-filled data. The current approach to gap filling in `neonSoilFlux`
359 uses monthly mean data to gap fill—this approach decreases the ability of the estimate to
360 be responsive to short-term pulses that occur with rapid weather shifts. All sites had more
361 than 75% of half-hourly periods with no-gap filled measurements (Figure S1, Supplementary
362 Information). At five out of six sites (all except SRER), we used at least some gap-filled
363 measurements of Soil Water Content (SWC). At WREF, field data collection occurred following

364 a severe rainstorm, with soils at the beginning of the sampling week near their water holding
365 capacity, which can influence the soil moisture sensor accuracy. In general, we recommend that
366 whenever possible, knowledge of local field conditions should influence analysis decisions in
367 addition to any QA filtering protocols in the `neonSoilFlux` package.

368 We recognize that this gap-filling approach may lead to gap-filled values that are quite different
369 from the actual values, such as an underestimate of soil moisture following rain events. Further
370 extensions of the gap filling method could use more sophisticated gap-filling routines, similar to
371 what is used for net ecosystem carbon exchange (Falge et al., 2001; Liu et al., 2023; Mariethoz
372 et al., 2015; Moffat et al., 2007; Zhang et al., 2023). Additionally, since the deepest temperature
373 and soil moisture sensors are located below the deepest CO₂ sensors at NEON sites, it is
374 possible that excluding these deeper layers from consideration prior to analysis would lead to a
375 reduced need for gap filling. Future iterations of the `neonSoilFlux` package may incorporate
376 this as an option. The current gap-filling routine provides a consistent approach that can be
377 applied to each data stream, but further work may explore alternative gap-filling approaches.

378 **5.2 Evaluation of flux-gradient approach at each site**

379 Derived results from the `neonSoilFlux` package have patterns that are broadly consistent with
380 those directly measured in the field (Figure 4 and Figure 5), even though statistical comparisons
381 between the field-measured and `neonSoilFlux` values were quite variable (e.g. R^2 ranging
382 from 0.12 to 0.77; Figure 6). One advantage of the `neonSoilFlux` package is its ability to
383 calculate fluxes across different soil depths (Figure 3), which allows for additional site-specific
384 customization. We believe the package can provide a useful baseline estimate of soil fluxes that
385 can always be complemented through additional field measurements.

386 The six locations studied provide a range of case studies that suggest different considerations

may apply to different sites when applying the flux-gradient method. For example, the Santa Rita Experimental Range (SRER) is a desert site characterized by sandy soil, which also was the location of the highest field soil temperatures that we observed (Table 2). At SRER the flux across the top two layers (F_{110}) produced a pattern of soil flux most consistent with the observed field data. The remaining methods F_{101} , F_{011} , or F_{000} are derived from information taken from the deepest layer, which seems to have been decoupled from the surface layers both in terms of temperature and CO₂ concentration. This may be a general circumstance where there are large diurnal temperature extremes that rapidly change during the course of a day and overnight, leading to lags in the timing of when temperature increases propagate down to deeper soil layers.

Immediately prior to our visit to Konza Prairie (KONZ), that site that experienced a significant rain event that led to wet soils that gradually dried out over the course of our time there. This pulse of precipitation increased the soil CO₂ concentration at the top layer above the concentrations in lower layers, leading to negative estimated flux values at the start of the field sampling period. In this case it was only when the soil began to return to a baseline level that the assumptions of the flux-gradient method were again met.

Both of the previous cases also provide context for the variable statistical comparisons between field-measured soil fluxes and `neonSoilFlux` outputs (Figure 6). When considering systematic deployment of this method across a measurement network, there are a number of independent challenges that require careful consideration. There are clear tradeoffs between (1) accuracy of modeled fluxes (defined here as closeness to field-measured F_S and the uncertainty reduction factor ϵ), (2) precision (which could be defined by the signal to noise ratio), and (3) the choice of the diffusivity model (Section 3.2.2) or flux computation method (Section 3.2.3). We performed a sensitivity analysis to compare the impact of these factors (Figure S2, Supplemental Information).

Finally, comparing the effects of different diffusivity estimation methods on the match between modeled and measured fluxes (Figure 5) highlights the sensitivity of F_{ijk} to diffusivity. The comparison between diffusivity estimates compared to field estimated diffusivity (Figure 7) demonstrates that site parameters can dictate which measure of diffusivity is most likely to be accurate in a given environmental context. Site-specific differences are largely a reflection of differences in soil moisture across the sites (Table 1), as not all diffusivity estimation methods incorporate soil moisture equivalently. While we here have compares two approaches to calculate diffusivity (the Millington-Quirk and Marshall models), it may be valuable to evaluate other diffusivity models (e.g. the Moldrup model; Moldrup et al. (1999)) as well. Ultimately the choice of a particular diffusivity model could be determined based on knowledge of site-specific evaluations or a set of these models could be used to generate a model ensemble average as a means to trade precision for a more general approach.

5.3 Recommendations for future method development

The `neonSoilFlux` package provides several approaches to estimate soil flux using the gradient method. We believe these approaches enable the software to be used across a range of site-specific assumptions (Maier & Schack-Kirchner, 2014). We note, however, that this choice can have a determinative approach on the calculated values. Ensemble averaging approaches (Elshall et al., 2018; Raftery et al., 2005) may be one way to address this problem if the goal is to calculate fluxes using the same method at a diverse range of different sites. Two other ideas would be to apply machine learning algorithms (*e.g.* random forest) to generate a single flux estimate across diverse sites, or using co-located estimates of net ecosystem carbon exchange from eddy-flux towers to further constrain results or to assess soil flux results for plausibility (Phillips et al., 2017).

These challenges notwithstanding, the method used here and made available in the

436 `neonSoilFlux` R package has the potential to produce nearly continuous estimates of flux
437 across all terrestrial NEON sites. These estimates are a significant improvement on available
438 approaches to constrain the portion of ecosystem respiration attributable to the soil. This, in
439 turn, also aids in our ability to understand the soil contribution to the net ecosystem flux
440 measured at these sites using the co-located eddy flux towers.

441 **6 Conclusions**

442 We used the R package `neonSoilFlux` to estimate soil CO₂ fluxes with the flux-gradient method
443 using data from buried soil sensors at NEON terrestrial sites. We compared the predicted
444 fluxes to those measured directly using a field-based closed chamber approach. Soil fluxes
445 from `neonSoilFlux` were broadly effective at producing estimates of flux comparable to those
446 measured in the field using a chamber-based technique. However `neonSoilFlux` outputs are
447 quite sensitive to a number of issues, including: missing data (and thus gap-filling of input
448 measurement datasets), the selection of soil depths used to best calculate the gradient (which
449 may vary between sites), and finally the choice of method used for estimating soil diffusivity.
450 The flexibility of the `neonSoilFlux` package allows the user to evaluate each of these issues
451 with site-specific knowledge and contexts. Future refinements and subsequent validation of
452 `neonSoilFlux` outputs will feed forward into evaluating soil carbon fluxes broader spatial scales
453 to enhance understanding of the ways in which soils across diverse ecosystems are responding
454 to a changing climate.

455 **Sources Cited**

- 456 Ayres, E., Reichle, R. H., Colliander, A., Cosh, M. H., & Smith, L. (2024). Validation of
457 Remotely Sensed and Modeled Soil Moisture at Forested and Unforested NEON Sites.
458 *IEEE Journal of Selected Topics in Applied Earth Observations and Remote Sensing*, 17,
459 14248–14264. <https://doi.org/10.1109/JSTARS.2024.3430928>
- 460 Baldocchi, D. (2014). Measuring fluxes of trace gases and energy between ecosystems and the
461 atmosphere - the state and future of the eddy covariance method. *Global Change Biology*,
462 20(12), 3600–3609. <https://doi.org/10.1111/gcb.12649>
- 463 Berenbaum, M. R., Carpenter, S. R., Hampton, S. E., Running, S. W., & Stanzione, D. C.
464 (2015). *Report from the NSF BIO Advisory Committee Subcommittee on NEON Scope
465 Impacts*.
- 466 Bond-Lamberty, B. (2018). New Techniques and Data for Understanding the Global Soil
467 Respiration Flux. *Earth's Future*, 6(9), 1176–1180. <https://doi.org/10.1029/2018EF000866>
- 468 Bond-Lamberty, B., Ballantyne, A., Berryman, E., Fluet-Chouinard, E., Jian, J., Morris, K.
469 A., Rey, A., & Vargas, R. (2024). Twenty Years of Progress, Challenges, and Opportunities
470 in Measuring and Understanding Soil Respiration. *Journal of Geophysical Research: Biogeosciences*, 129(2), e2023JG007637. <https://doi.org/10.1029/2023JG007637>
- 472 Bond-Lamberty, B., Christianson, D. S., Malhotra, A., Pennington, S. C., Sihi, D., AghaK-
473 ouchak, A., Anjileli, H., Altaf Arain, M., Armesto, J. J., Ashraf, S., Ataka, M., Baldocchi,
474 D., Andrew Black, T., Buchmann, N., Carbone, M. S., Chang, S.-C., Crill, P., Curtis, P.
475 S., Davidson, E. A., ... Zou, J. (2020). COSORE: A community database for continuous
476 soil respiration and other soil-atmosphere greenhouse gas flux data. *Global Change Biology*,
477 26(12), 7268–7283. <https://doi.org/10.1111/gcb.15353>
- 478 Bond-Lamberty, B., & Thomson, A. (2010). A global database of soil respiration data.
479 *Biogeosciences*, 7(6), 1915–1926. <https://doi.org/10.5194/bg-7-1915-2010>

- 480 Bond-Lamberty, B., Wang, C., & Gower, S. T. (2004). A global relationship between the
481 heterotrophic and autotrophic components of soil respiration? *Global Change Biology*,
482 10(10), 1756–1766. <https://doi.org/10.1111/j.1365-2486.2004.00816.x>
- 483 Bouma, T. J., & Bryla, D. R. (2000). On the assessment of root and soil respiration for soils of
484 different textures: Interactions with soil moisture contents and soil CO₂ concentrations.
485 *Plant and Soil*, 227(1), 215–221. <https://doi.org/10.1023/A:1026502414977>
- 486 Chen, H., & Tian, H.-Q. (2005). Does a General Temperature-Dependent Q10 Model of Soil
487 Respiration Exist at Biome and Global Scale? *Journal of Integrative Plant Biology*, 47(11),
488 1288–1302. <https://doi.org/10.1111/j.1744-7909.2005.00211.x>
- 489 Davidson, E. A., Janssens, I. A., & Luo, Y. (2006). On the variability of respiration in
490 terrestrial ecosystems: Moving beyond Q10. *Global Change Biology*, 12, 154–164. <https://doi.org/10.1111/j.1365-2486.2005.01065.x>
- 491 Desai, A. R., Murphy, B. A., Wiesner, S., Thom, J., Butterworth, B. J., Koupaei-Abyazani, N.,
492 Muttaqin, A., Paleri, S., Talib, A., Turner, J., Mineau, J., Merrelli, A., Stoy, P., & Davis,
493 K. (2022). Drivers of Decadal Carbon Fluxes Across Temperate Ecosystems. *Journal of
494 Geophysical Research: Biogeosciences*, 127(12), e2022JG007014. <https://doi.org/10.1029/2022JG007014>
- 495 Efron, B., & Tibshirani, R. J. (1994). *An Introduction to the Bootstrap*. Chapman and
496 Hall/CRC. <https://doi.org/10.1201/9780429246593>
- 497 Elshall, A. S., Ye, M., Pei, Y., Zhang, F., Niu, G.-Y., & Barron-Gafford, G. A. (2018). Relative
498 model score: A scoring rule for evaluating ensemble simulations with application to microbial
499 soil respiration modeling. *Stochastic Environmental Research and Risk Assessment*, 32(10),
500 2809–2819. <https://doi.org/10.1007/s00477-018-1592-3>
- 501 Falge, E., Baldocchi, D., Olson, R., Anthoni, P., Aubinet, M., Bernhofer, C., Burba, G.,
502 Ceulemans, R., Clement, R., Dolman, H., Granier, A., Gross, P., Grünwald, T., Hollinger,
503 D., Jensen, N.-O., Katul, G., Keronen, P., Kowalski, A., Lai, C. T., ... Wofsy, S. (2001).

- 506 Gap filling strategies for defensible annual sums of net ecosystem exchange. *Agricultural*
507 and *Forest Meteorology*, 107(1), 43–69. [https://doi.org/10.1016/S0168-1923\(00\)00225-2](https://doi.org/10.1016/S0168-1923(00)00225-2)
- 508 Farrance, I., & Frenkel, R. (2012). *Uncertainty of Measurement: A Review of the Rules*
509 for Calculating Uncertainty Components through Functional Relationships. *The Clinical*
510 *Biochemist Reviews*, 33(2), 49–75.
- 511 Friedlingstein, P., O’Sullivan, M., Jones, M. W., Andrew, R. M., Hauck, J., Landschützer,
512 P., Le Quéré, C., Li, H., Luijckx, I. T., Olsen, A., Peters, G. P., Peters, W., Pongratz,
513 J., Schwingshackl, C., Sitch, S., Canadell, J. G., Ciais, P., Jackson, R. B., Alin, S. R., ...
514 Zeng, J. (2025). Global Carbon Budget 2024. *Earth System Science Data*, 17(3), 965–1039.
515 <https://doi.org/10.5194/essd-17-965-2025>
- 516 Hamdi, S., Moyano, F., Sall, S., Bernoux, M., & Chevallier, T. (2013). Synthesis analysis
517 of the temperature sensitivity of soil respiration from laboratory studies in relation to
518 incubation methods and soil conditions. *Soil Biology and Biochemistry*, 58, 115–126.
519 <https://doi.org/10.1016/j.soilbio.2012.11.012>
- 520 Jackson, R. B., Lajtha, K., Crow, S. E., Hugelius, G., Kramer, M. G., & Piñeiro, G. (2017).
521 The Ecology of Soil Carbon: Pools, Vulnerabilities, and Biotic and Abiotic Controls.
522 *Annual Review of Ecology, Evolution and Systematics*, 48(Volume 48, 2017), 419–445.
523 <https://doi.org/10.1146/annurev-ecolsys-112414-054234>
- 524 Jian, J., Bailey, V., Dorheim, K., Konings, A. G., Hao, D., Shiklomanov, A. N., Snyder,
525 A., Steele, M., Teramoto, M., Vargas, R., & Bond-Lamberty, B. (2022). Historically
526 inconsistent productivity and respiration fluxes in the global terrestrial carbon cycle. *Nature*
527 *Communications*, 13(1), 1733. <https://doi.org/10.1038/s41467-022-29391-5>
- 528 Jian, J., Vargas, R., Anderson-Teixeira, K., Stell, E., Herrmann, V., Horn, M., Kholod, N.,
529 Manzon, J., Marchesi, R., Paredes, D., & Bond-Lamberty, B. (2021). A restructured and
530 updated global soil respiration database (SRDB-V5). *Earth System Science Data*, 13(2),
531 255–267. <https://doi.org/10.5194/essd-13-255-2021>

- 532 Jiang, J., Feng, L., Hu, J., Liu, H., Zhu, C., Chen, B., & Chen, T. (2024). Global soil
533 respiration predictions with associated uncertainties from different spatio-temporal data
534 subsets. *Ecological Informatics*, 82, 102777. <https://doi.org/10.1016/j.ecoinf.2024.102777>
- 535 Jobbágy, E. G., & Jackson, R. B. (2000). The Vertical Distribution of Soil Organic Carbon
536 and its Relation to Climate and Vegetation. *Ecological Applications*, 10(2), 423–436.
537 [https://doi.org/10.1890/1051-0761\(2000\)010%5B0423:TVDOSO%5D2.0.CO;2](https://doi.org/10.1890/1051-0761(2000)010%5B0423:TVDOSO%5D2.0.CO;2)
- 538 Jurasinski, G., Koebisch, F., Guenther, A., & Beetz, S. (2022). *Flux: Flux Rate Calculation
539 from Dynamic Closed Chamber Measurements*.
- 540 Liu, K., Li, X., Wang, S., & Zhang, H. (2023). A robust gap-filling approach for European
541 Space Agency Climate Change Initiative (ESA CCI) soil moisture integrating satellite
542 observations, model-driven knowledge, and spatiotemporal machine learning. *Hydrology
543 and Earth System Sciences*, 27(2), 577–598. <https://doi.org/10.5194/hess-27-577-2023>
- 544 Lunch, C., Laney, C., Mietkiewicz, N., Sokol, E., Cawley, K., & Network), N. (National. E. O.
545 (2025). *neonUtilities: Utilities for Working with NEON Data*.
- 546 Luo, Y., Ogle, K., Tucker, C., Fei, S., Gao, C., LaDeau, S., Clark, J. S., & Schimel, D. S. (2011).
547 Ecological forecasting and data assimilation in a data-rich era. *Ecological Applications*,
548 21(5), 1429–1442. <https://doi.org/10.1890/09-1275.1>
- 549 Maier, M., & Schack-Kirchner, H. (2014). Using the gradient method to determine soil gas
550 flux: A review. *Agricultural and Forest Meteorology*, 192–193, 78–95. <https://doi.org/10.1016/j.agrformet.2014.03.006>
- 552 Mariethoz, G., Linde, N., Jougnot, D., & Rezaee, H. (2015). Feature-preserving interpolation
553 and filtering of environmental time series. *Environmental Modelling & Software*, 72, 71–76.
554 <https://doi.org/10.1016/j.envsoft.2015.07.001>
- 555 Marshall, T. J. (1959). The Diffusion of Gases Through Porous Media. *Journal of Soil Science*,
556 10(1), 79–82. <https://doi.org/10.1111/j.1365-2389.1959.tb00667.x>
- 557 Millington, R. J., & Shearer, R. C. (1971). Diffusion in aggregated porous media. *Soil Science*,

- 558 111(6), 372–378.
- 559 Moffat, A. M., Papale, D., Reichstein, M., Hollinger, D. Y., Richardson, A. D., Barr, A. G.,
560 Beckstein, C., Braswell, B. H., Churkina, G., Desai, A. R., Falge, E., Gove, J. H., Heimann,
561 M., Hui, D., Jarvis, A. J., Kattge, J., Noormets, A., & Stauch, V. J. (2007). Comprehensive
562 comparison of gap-filling techniques for eddy covariance net carbon fluxes. *Agricultural and*
563 *Forest Meteorology*, 147(3), 209–232. <https://doi.org/10.1016/j.agrformet.2007.08.011>
- 564 Moldrup, P., Olesen, T., Yamaguchi, T., Schjønning, P., & Rolston, D. E. (1999). Modeling
565 diffusion and reaction in soils: 9. The Buckingham-Burdine-Campbell equation for gas
566 diffusivity in undisturbed soil. *Soil Science*, 164(2), 75.
- 567 NEON. (2024a). *Barometric pressure (DP1.00004.001)*. National Ecological Observatory
568 Network (NEON). <https://doi.org/10.48443/RT4V-KZ04>
- 569 NEON. (2024b). *Soil CO₂ concentration (DP1.00095.001)*. National Ecological Observatory
570 Network (NEON). <https://doi.org/10.48443/E7GR-6G94>
- 571 NEON. (2024c). *Soil physical and chemical properties, Megapit (DP1.00096.001)*. National
572 Ecological Observatory Network (NEON). <https://doi.org/10.48443/S6ND-Q840>
- 573 NEON. (2024d). *Soil temperature (DP1.00041.001)*. National Ecological Observatory Network
574 (NEON). <https://doi.org/10.48443/Q24X-PW21>
- 575 NEON. (2024e). *Soil water content and water salinity (DP1.00094.001)*. National Ecological
576 Observatory Network (NEON). <https://doi.org/10.48443/A8VY-Y813>
- 577 Norman, J. M., Kucharik, C. J., Gower, S. T., Baldocchi, D. D., Crill, P. M., Rayment,
578 M., Savage, K., & Striegl, R. G. (1997). A comparison of six methods for measuring
579 soil-surface carbon dioxide fluxes. *Journal of Geophysical Research: Atmospheres*, 102(D24),
580 28771–28777. <https://doi.org/10.1029/97JD01440>
- 581 Pedersen, A. R. (2024). *HMR: Flux Estimation with Static Chamber Data*.
- 582 Phillips, C. L., Bond-Lamberty, B., Desai, A. R., Lavoie, M., Risk, D., Tang, J., Todd-Brown,
583 K., & Vargas, R. (2017). The value of soil respiration measurements for interpreting and

- 584 modeling terrestrial carbon cycling. *Plant and Soil*, 413(1), 1–25. <https://doi.org/10.1007/s11104-016-3084-x>
- 585
- 586 Raftery, A. E., Gneiting, T., Balabdaoui, F., & Polakowski, M. (2005). *Using Bayesian Model*
587 *Averaging to Calibrate Forecast Ensembles*. <https://doi.org/10.1175/MWR2906.1>
- 588 Rheault, K., Christiansen, J. R., & Larsen, K. S. (2024). goFlux: A user-friendly way to
589 calculate GHG fluxes yourself, regardless of user experience. *Journal of Open Source*
590 *Software*, 9(96), 6393. <https://doi.org/10.21105/joss.06393>
- 591 Sallam, A., Jury, W. A., & Letey, J. (1984). Measurement of Gas Diffusion Coefficient under
592 Relatively Low Air-filled Porosity. *Soil Science Society of America Journal*, 48(1), 3–6.
593 <https://doi.org/10.2136/sssaj1984.03615995004800010001x>
- 594 Shao, J., Zhou, X., Luo, Y., Li, B., Aurela, M., Billesbach, D., Blanken, P. D., Bracho, R.,
595 Chen, J., Fischer, M., Fu, Y., Gu, L., Han, S., He, Y., Kolb, T., Li, Y., Nagy, Z., Niu, S.,
596 Oechel, W. C., ... Zhang, J. (2015). Biotic and climatic controls on interannual variability
597 in carbon fluxes across terrestrial ecosystems. *Agricultural and Forest Meteorology*, 205,
598 11–22. <https://doi.org/10.1016/j.agrformet.2015.02.007>
- 599 Shao, P., Zeng, X., Moore, D. J. P., & Zeng, X. (2013). Soil microbial respiration from
600 observations and Earth System Models. *Environmental Research Letters*, 8(3), 034034.
601 <https://doi.org/10.1088/1748-9326/8/3/034034>
- 602 Sihi, D., Gerber, S., Inglett, P. W., & Inglett, K. S. (2016). Comparing models of microbial–
603 substrate interactions and their response to warming. *Biogeosciences*, 13(6), 1733–1752.
604 <https://doi.org/10.5194/bg-13-1733-2016>
- 605 Tang, J., Baldocchi, D. D., Qi, Y., & Xu, L. (2003). Assessing soil CO₂ efflux using continuous
606 measurements of CO₂ profiles in soils with small solid-state sensors. *Agricultural and Forest*
607 *Meteorology*, 118(3), 207–220. [https://doi.org/10.1016/S0168-1923\(03\)00112-6](https://doi.org/10.1016/S0168-1923(03)00112-6)
- 608 Tang, J., Misson, L., Gershenson, A., Cheng, W., & Goldstein, A. H. (2005). Continuous
609 measurements of soil respiration with and without roots in a ponderosa pine plantation

- 610 in the Sierra Nevada Mountains. *Agricultural and Forest Meteorology*, 132(3), 212–227.
611 <https://doi.org/10.1016/j.agrformet.2005.07.011>
- 612 Taylor, J. R. (2022). *An Introduction to Error Analysis: The Study of Uncertainties in Physical*
613 *Measurements, Third Edition* (3rd ed.). University Science Press.
- 614 Wilson, S. J., Bond-Lamberty, B., Noyce, G., Bittencourt Peixoto, R., & Megonigal, J. P.
615 (2024). Fluxfinder: An R Package for Reproducible Calculation and Initial Processing
616 of Greenhouse Gas Fluxes From Static Chamber Measurements. *Journal of Geophysical*
617 *Research: Biogeosciences*, 129(11), e2024JG008208. <https://doi.org/10.1029/2024JG008208>
- 618 Yan, Z., Bond-Lamberty, B., Todd-Brown, K. E., Bailey, V. L., Li, S., Liu, C., & Liu, C. (2018).
619 A moisture function of soil heterotrophic respiration that incorporates microscale processes.
620 *Nature Communications*, 9(1), 2562. <https://doi.org/10.1038/s41467-018-04971-6>
- 621 Yan, Z., Liu, C., Todd-Brown, K. E., Liu, Y., Bond-Lamberty, B., & Bailey, V. L. (2016).
622 Pore-scale investigation on the response of heterotrophic respiration to moisture conditions
623 in heterogeneous soils. *Biogeochemistry*, 131(1), 121–134. <https://doi.org/10.1007/s10533-016-0270-0>
- 625 Zhang, R., Kim, S., Kim, H., Fang, B., Sharma, A., & Lakshmi, V. (2023). Temporal Gap-Filling
626 of 12-Hourly SMAP Soil Moisture Over the CONUS Using Water Balance Budgeting. *Water*
627 *Resources Research*, 59(12), e2023WR034457. <https://doi.org/10.1029/2023WR034457>
- 628 Zhao, J. (2019). FluxCalR: A R package for calculating CO₂ and CH₄ fluxes from static
629 chambers. *Journal of Open Source Software*, 4(43), 1751. <https://doi.org/10.21105/joss.01751>
- 631 Zobitz, J., Ayres, E., O'Rourke, K., Werbin, Z., Lee, L., Abdi, R., Mehmeti, D., & Xiong, L.
632 (2024). *neonSoilFlux: Compute Soil Carbon Fluxes for the National Ecological Observatory*
633 *Network Sites*.
- 634 Zobitz, J., & Zimmerman, N. (2025). *Supporting Code and Data for neonSoilFlux: An R*
635 *Package for Continuous Sensor-Based Estimation of Soil CO₂ Fluxes*. Zenodo. <https://doi.org/10.5281/zenodo.5520220>

636 //doi.org/10.5281/zenodo.17516320